



Dynamic modeling and analysis on rigid-flexible coupling between vertical chatter and transverse bending vibration in process of cold rolling

Xiao-yong Wang¹ · Zhi-ying Gao¹ · Yan-li Xin¹ · Qing-dong Zhang¹

Received: 7 October 2023 / Revised: 6 November 2023 / Accepted: 9 November 2023
© China Iron and Steel Research Institute Group Co., Ltd. 2024

Abstract

Considering the dynamic variation of roll gap and the transverse distribution of dynamic rolling force along the work roll width direction, the movement and deformation of rolls system, influenced by the coupling of vertical chatter and transverse bending vibration, may cause instability and also bring product defect of thickness difference. Therefore, a rigid-flexible coupling vibration model of the rolls system was presented. The influence of dynamic characteristics on the rolling process stability and strip thickness distribution was investigated. Firstly, assuming the symmetry of upper and lower structures of six-high rolling mill, a transverse bending vibration model of three-beam system under simply supported boundary conditions was established, and a semi-analytical solution method was proposed to deal with this model. Then, considering both variation and change rate of the roll gap, a roll vertical chatter model with structure and process coupled was constructed, and the critical rolling speed for self-excited instability was determined by Routh stability criterion. Furthermore, a rigid-flexible coupling vibration model of the rolls system was built by connecting the vertical chatter model and transverse bending vibration model through the distribution of dynamic rolling force, and the dynamic characteristics of rolls system were analyzed. Finally, the strip exit thickness distributions under the stable and unstable rolling process were compared, and the product shape and thickness distribution characteristics were quantitatively evaluated by the crown and maximum longitudinal thickness difference.

Keywords Transverse bending vibration · Vertical chatter · Rigid-flexible coupling vibration · Strip thickness distribution · Rolling process stability

1 Introduction

With the increasing demand for high-precision strip products, ensuring the strip products quality under the premise of rolling equipment stable operation is getting more and more attention and has become the primary task. The movement and deformation of rolls systems caused by vertical chatter and transverse bending vibration are two important factors that affect the quality of strip products. Roll vertical chatter may not only cause the strip thickness difference along the rolling direction (longitudinal

thickness difference) and surface vibration mark, but also lead to the rolling process instability. In particular, when the chatter is serious, it may cause production stop or strip-breaking accident. The strip profile is determined by the shape of loaded roll gap, and the transverse bending vibration of rolls system affects the shape of roll gap. Therefore, irregular or excessive roll deformation caused by transverse bending vibration will cause strip thickness difference along the strip width direction (transverse thickness difference) and flatness defect.

The research approaches for roll vertical chatter mainly include finite element method and lumped mass method. Although the finite element method [1–7] is suitable for analyzing the modal characteristics of vibration, it is difficult to present the analytical rules related to the rolling process, and it has the problem of long computing time. Therefore, lumped mass method is still more widely used

✉ Zhi-ying Gao
gaozhiying@me.ustb.edu.cn

¹ School of Mechanical Engineering, University of Science and Technology Beijing, Beijing 100083, China

in rolling mill vertical chatter modeling. In recent years, scholars have combined this method with the knowledge of rolling process mechanism for the purpose of explaining chatter phenomena, discovering chatter mechanism, and providing suppression measures.

Liu et al. [8] investigated the effect of different factors on the stability of tandem rolling mills and revealed the mechanism of regenerative chatter. Zeng et al. [9] suggested a vertical–torsional–horizontal coupling chatter model and analyzed the system stability based on Routh criterion. Gao et al. [10] established a dynamic model of cold rolling with structure–process–control coupled and put forward a definition of critical rolling speed to predict and suppress chatter. Lu et al. [11] proposed a time-varying stability criterion to evaluate mill stability and made optimal design of rolling reduction and friction. Gao et al. [12] proposed a dynamics-based optimization model of rolling schedule for the 5-stand cold tandem system through combining the critical rolling speeds with the system dynamic behavior. The friction and lubrication condition of roll gap is one of the important factors affecting chatter, and the establishment of a reasonable friction model is the key premise for accurate chatter modeling. Heidari et al. [13] proposed a chatter model of the cold rolling with consideration of unsteady lubrication and investigated the influence of lubrication parameters on critical rolling speed. Fujita et al. [14] investigated the effect of lubrication properties on the oil film and realized the dynamic control of friction coefficient in a tandem rolling mill based on self-excited vibration model. Cao et al. [15] proposed a new dynamic rolling model and studied the changes of parameters such as neutral angle and lubrication state during vibration. These theoretical research results are of great value for revealing chatter mechanism and providing suppression strategies. However, the lumped mass model assumes that the roll and stand are lumped mass blocks, and mainly studies the influence of vertical chatter on the strip longitudinal thickness difference that is essentially the two-dimensional model. It is difficult to reflect the information of roll transverse direction and strip width direction.

The problem of roll transverse deformation is important in the study of strip shape, because roll transverse deformation directly affects the strip profile after rolling. Solving the roll deformation is the premise of accurately predicting the strip profile and stress distribution under specific rolling process conditions. The commonly used methods for solving roll deformation problems include analytical method [16], influence function method [17–20], and finite element method [21, 22]. However, most of the above methods are based on statics theory, and the dynamic response of roll deformation with time cannot be obtained. They also have some shortcomings, such as low calculation accuracy, difficult convergence, and long

calculation time. Therefore, the methods for solving roll deformation are gradually developing toward dynamic, efficient, and accurate.

Considering the symmetry of the upper and lower rolls system, Sun et al. [23] studied a four-high rolling mill by simplifying the rolls system as simply supported double-beam system. The dynamic characteristics of rolls system transverse bending vibration were analyzed, including the free transverse vibration characteristics [24] and forced transverse vibration response under different forms of rolling force [25]. Finally, the rolls system transverse bending vibration model and the rolling process model were coupled and modified [26]. The changes of parameters such as strip profile and stress distribution with time during stable rolling process were obtained. However, the analytical method used in the above research is only suitable for the simply supported double-beam system corresponding to the four-high rolling mill. Therefore, the problem of expanding the model application scope can be further studied, such as applying the model to the six-high rolling mill or other more complex boundary conditions. In addition, the roll vertical chatter can be further considered. Kapil et al. [27] discretized the roll into Euler–Bernoulli beam elements, used the displacement and velocity of element nodes to predict the strip thickness and profile, and studied the influence of support stiffness on strip crown. The dynamic model could predict the strip profile and stress distribution, which is helpful to avoid flatness defects in the rolling process. Malik and Grandhi [28, 29] proposed a new finite element method which can rapidly calculate the mill deflection and strip profile. In this method, the roll and strip are discretized into Timoshenko beam elements. In subsequent research, Malik and Hinton [30], Zhang and Malik [31, 32], and Patel et al. [33] further considered the influence of roll crown, strip crown, roll surface roughness, and roll grinding error. However, the above method is still a static method, and the dynamic response of the rolls system cannot be obtained. Thus, Patel et al. [34] extended the static model to a dynamic model and applied the dynamic model in different rolling mills. However, because the strip was simplified to strip modulus, the above dynamic model did not take into account the influence of dynamic rolling process model.

In this paper, the influence of coupling between rolls system vertical chatter and transverse bending vibration on strip thickness distribution and rolling process stability is studied. Firstly, considering the symmetry of the upper and lower rolls system, the six-high rolling mill is simplified to the three-beam system under simply supported boundary conditions, and a semi-analytical method is proposed to solve the transverse bending vibration of the rolls system. The correctness of the model is verified by comparing the calculation results from the analytical method. Then, the roll vertical chatter model with structure–process coupled is

applied, and the critical rolling speed is obtained based on the Routh stability criterion. The simulation results calculated by the model are very close to the experimental results. Furthermore, the rolls system vertical chatter model and transverse bending vibration model are coupled through the dynamic rolling force, and the rigid-flexible coupling vibration model is constructed. The proposed semi-analytical method is applied to obtain the free transverse vibration modal characteristics of the rolls system, and the forced vibration responses of the rolls system under dynamic rolling force are obtained. Finally, the strip exit thickness distributions under stable and unstable rolling processes are compared and analyzed. The thickness distribution is further quantified by the crown and maximum longitudinal thickness difference. The results show that the rolls system rigid-flexible coupling vibration model can accurately describe the movement and deformation behavior of the rolls system. The rolls system dynamic responses under different rolling conditions and the strip product quality information along rolling direction and width direction are discussed.

2 Rolls system rigid-flexible coupling vibration model

2.1 Rolls system transverse bending vibration model

2.1.1 Model construction

Taking into account the symmetry of the upper and lower rolls system, the six-high rolling mill can be simplified to a simply supported three-beam system, as illustrated in Fig. 1. The rolls are connected by uniformly-distributed connecting elastic layer K . Furthermore, both rolls are homogeneous and have the same length L , but they may have different mass densities or flexural rigidities.

Based on the Bernoulli–Euler beam theory, the transverse bending vibration of the rolls system in a six-high rolling mill is described by the following governing equation of motion:

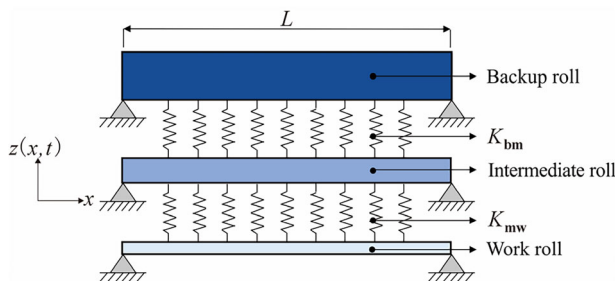


Fig. 1 Rolls system transverse bending vibration model of six-high rolling mill

$$\begin{cases} \rho_b S_b \frac{\partial^2 z_b}{\partial t^2} + E_b I_b \frac{\partial^4 z_b}{\partial x^4} + K_{bm}(z_b - z_m) = f_b(x, t) \\ \rho_m S_m \frac{\partial^2 z_m}{\partial t^2} + E_m I_m \frac{\partial^4 z_m}{\partial x^4} - K_{bm}(z_b - z_m) + K_{mw}(z_m - z_w) = f_m(x, t) \\ \rho_w S_w \frac{\partial^2 z_w}{\partial t^2} + E_w I_w \frac{\partial^4 z_w}{\partial x^4} - K_{mw}(z_m - z_w) = f_w(x, t) \end{cases} \quad (1)$$

where x and t represent the spatial and time coordinate; $z = z(x, t)$ denotes the transverse deflection; subscripts b, m, and w represent the backup roll, intermediate roll, and work roll, respectively; E is the Young’s moduli; I is the inertia moment; ρ is the mass density; S is the cross-section area; K_{bm} is the stiffness modulus of the elastic layer between backup roll and intermediate roll; K_{mw} is the stiffness modulus of the elastic layer between intermediate roll and work roll; and $f(x, t)$ is the exciting force. With the assumption of $E_i I_i = e_i$ and $\rho_i S_i = \bar{m}_i$ ($i = b, m, w$), Eq. (1) is transformed into the following form:

$$\begin{cases} \bar{m}_b \frac{\partial^2 z_b}{\partial t^2} + e_b \frac{\partial^4 z_b}{\partial x^4} + K_{bm}(z_b - z_m) = f_b(x, t) \\ \bar{m}_m \frac{\partial^2 z_m}{\partial t^2} + e_m \frac{\partial^4 z_m}{\partial x^4} - K_{bm}(z_b - z_m) + K_{mw}(z_m - z_w) = f_m(x, t) \\ \bar{m}_w \frac{\partial^2 z_w}{\partial t^2} + e_w \frac{\partial^4 z_w}{\partial x^4} - K_{mw}(z_m - z_w) = f_w(x, t) \end{cases} \quad (2)$$

where e_i is the flexural rigidity of different rolls; and \bar{m}_i is the mass of per unit length of different rolls. The boundary conditions of the simply supported beam are as follows:

$$z_i(0, t) = z_i(L, t) = \frac{\partial^2 z_i(0, t)}{\partial x^2} = \frac{\partial^2 z_i(L, t)}{\partial x^2} = 0 \quad (3)$$

The solution method for rolls system transverse bending vibration can be divided into two parts: (1) The rolls system free transverse vibration is solved based on semi-analytical method to obtain the natural frequencies and mode shapes. (2) Based on the orthogonality condition for different mode shapes, the unknown time function of the rolls system forced transverse vibration is solved. By combining with the natural frequencies and mode shapes obtained from the free transverse vibration, the rolls system transverse bending vibration response is obtained.

The solutions of the free transverse vibration are separable in time and space, and the solution can be assumed in the form as follows:

$$\begin{cases} z_b(x, t) = D e^{j\omega t} A e^{Px} \\ z_m(x, t) = D e^{j\omega t} B e^{Px} \\ z_w(x, t) = D e^{j\omega t} C e^{Px} \end{cases} \quad (4)$$

where $D e^{j\omega t}$ is the time function of free transverse vibration; $A e^{Px}$, $B e^{Px}$, and $C e^{Px}$ are the mode shape function of

the backup roll, intermediate roll, and work roll, respectively; ω is the natural frequency; A, B, C, D , and P are the unknown constants; and $j = \sqrt{-1}$ is the imaginary unit. Equation (4) is substituted into the free vibration form of Eq. (2), that is, the exciting force is equal to 0, and the following equations are obtained.

$$\begin{bmatrix} e_b P^4 + K_{bm} - \bar{m}_b \omega^2 & -K_{bm} & 0 \\ -K_{bm} & e_m P^4 + K_{bm} + K_{mw} - \bar{m}_m \omega^2 & -K_{mw} \\ 0 & -K_{mw} & e_w P^4 + K_{mw} - \bar{m}_w \omega^2 \end{bmatrix} \begin{Bmatrix} A \\ B \\ C \end{Bmatrix} = \begin{Bmatrix} 0 \\ 0 \\ 0 \end{Bmatrix} \quad (5)$$

The nontrivial solution for Eq. (5) requires that the determinant of the coefficient matrix equals to 0, which derives out a twelve-order polynomial equation in terms of P :

$$\begin{vmatrix} e_b P^4 + K_{bm} - \bar{m}_b \omega^2 & -K_{bm} & 0 \\ -K_{bm} & e_m P^4 + K_{bm} + K_{mw} - \bar{m}_m \omega^2 & -K_{mw} \\ 0 & -K_{mw} & e_w P^4 + K_{mw} - \bar{m}_w \omega^2 \end{vmatrix} = 0 \quad (6)$$

There are twelve roots P_k ($k = 1-12$) for Eq. (6), and by substituting P_k into Eq. (5), the relationship between unknown constants A, B , and C is obtained as follows:

$$\begin{cases} A_k = \beta_k B_k \\ C_k = \gamma_k B_k \\ \beta_k = \frac{K_{bm}}{e_b P_k^4 + K_{bm} - \bar{m}_b \omega^2} \\ \gamma_k = \frac{K_{mw}}{e_w P_k^4 + K_{mw} - \bar{m}_w \omega^2} \end{cases} \quad (7)$$

where A_k, B_k, C_k, β_k , and γ_k are the unknown constants corresponding to the root P_k . The roll transverse deflections of the six-high rolling mill under free transverse vibration can be obtained by substituting Eq. (7) into Eq. (4):

$$\begin{cases} z_b(x, t) = \sum_{n=1}^{\infty} D_n e^{j\omega_n t} \left[\sum_{k=1}^{12} \beta_{nk} B_{nk} e^{P_{nk} x} \right] = \sum_{n=1}^{\infty} D_n e^{j\omega_n t} \phi_{nb}(x) \\ z_m(x, t) = \sum_{n=1}^{\infty} D_n e^{j\omega_n t} \left[\sum_{k=1}^{12} B_{nk} e^{P_{nk} x} \right] = \sum_{n=1}^{\infty} D_n e^{j\omega_n t} \phi_{nm}(x) \\ z_w(x, t) = \sum_{n=1}^{\infty} D_n e^{j\omega_n t} \left[\sum_{k=1}^{12} \gamma_{nk} B_{nk} e^{P_{nk} x} \right] = \sum_{n=1}^{\infty} D_n e^{j\omega_n t} \phi_{nw}(x) \end{cases} \quad (8)$$

where ω_n is the n th natural frequency; $B_{nk}, \beta_{nk}, \gamma_{nk}, D_n$, and P_{nk} are the unknown constants corresponding to the n th natural frequency; and $\phi_{nb}(x), \phi_{nm}(x)$, and $\phi_{nw}(x)$ are the mode shape function of the backup roll, intermediate roll, and work roll corresponding to the n th natural frequency, respectively. Substituting the boundary conditions of Eq. (3) into Eq. (8), twelve equations for unknown constants B_{nk} ($k = 1-12$) under each natural frequency can be represented into matrix form as follows:

$$[E]_{12 \times 12} \{B\}_{12 \times 1} = \{0\}_{12 \times 1} \quad (9)$$

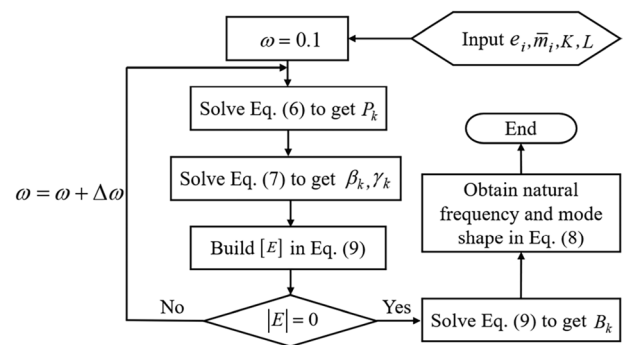


Fig. 2 Flowchart of semi-analytical method to determine natural frequencies and mode shape function

where $\{B\}_{12 \times 1}$ is the unknown constants vector; $\{0\}_{12 \times 1}$ is the zero vector; and $[E]_{12 \times 12}$ is the boundary conditions coefficient matrix. Nontrivial solutions for Eq. (9) will exist only when the determinant of the boundary conditions coefficient matrix $[E]_{12 \times 12}$ is equal to 0. Based on the above analysis, the natural frequency and mode shape function of transverse vibration can be determined by a semi-analytical method. The calculation process is shown in Fig. 2, and $\Delta\omega$ is the increment of natural frequency at each cycle. Once the frequency range is determined, all the natural frequencies and corresponding mode shapes in that range can be obtained by the semi-analytical method.

Before solving the rolls system forced transverse vibration, the orthogonality condition for different mode shapes should be obtained. Equation (2) for free transverse vibration ($f_i(x, t) = 0$) can be transformed into the following form:

$$\begin{cases} -\bar{m}_b \frac{\partial^2 z_b}{\partial t^2} = e_b \frac{\partial^4 z_b}{\partial x^4} + K_{bm}(z_b - z_m) \\ -\bar{m}_m \frac{\partial^2 z_m}{\partial t^2} = e_m \frac{\partial^4 z_m}{\partial x^4} - K_{bm}(z_b - z_m) + K_{mw}(z_m - z_w) \\ -\bar{m}_w \frac{\partial^2 z_w}{\partial t^2} = e_w \frac{\partial^4 z_w}{\partial x^4} - K_{mw}(z_m - z_w) \end{cases} \quad (10)$$

The left terms $-\bar{m}_b \frac{\partial^2 z_b}{\partial t^2}$, $-\bar{m}_m \frac{\partial^2 z_m}{\partial t^2}$, and $-\bar{m}_w \frac{\partial^2 z_w}{\partial t^2}$ can be treated as a kind of inertial force that is recorded as $f_{i1}(x, t)$, $f_{i2}(x, t)$, and $f_{i3}(x, t)$. The right terms can be treated as a sort of elastic force. Considering the whole three-beam system, an energy equilibrium equation can be obtained as follows:

$$\int_0^L [z_{bn}(x, t) f_{i1n}(x, t) + z_{mn}(x, t) f_{i2n}(x, t) + z_{wn}(x, t) f_{i3n}(x, t)] dx = \int_0^L [z_{bn}(x, t) f_{11m}(x, t) + z_{mn}(x, t) f_{12m}(x, t) + z_{wn}(x, t) f_{13m}(x, t)] dx \quad (11)$$

where m and n correspond to the m th and n th natural frequencies, respectively. Substituting Eq. (8) into Eq. (11), Eq. (11) is transformed into the following form:

$$\int_0^L [D_m e^{i\omega_n t} D_n e^{i\omega_n t} \phi_{mb}(x) \bar{m}_b \omega_n^2 \phi_{nb}(x) + D_m e^{i\omega_n t} D_n e^{i\omega_n t} \phi_{mm}(x) \bar{m}_m \omega_n^2 \phi_{nm}(x) + D_m e^{i\omega_n t} D_n e^{i\omega_n t} \phi_{mw}(x) \bar{m}_w \omega_n^2 \phi_{nw}(x)] dx = \int_0^L [D_n e^{i\omega_n t} D_m e^{i\omega_n t} \phi_{nb}(x) \bar{m}_b \omega_n^2 \phi_{mb}(x) + D_n e^{i\omega_n t} D_m e^{i\omega_n t} \phi_{nm}(x) \bar{m}_m \omega_n^2 \phi_{mm}(x) + D_n e^{i\omega_n t} D_m e^{i\omega_n t} \phi_{nw}(x) \bar{m}_w \omega_n^2 \phi_{mw}(x)] dx \tag{12}$$

Merging similar items, Eq. (12) can be simplified as follows:

$$\left\{ \int_0^L [\phi_{mb}(x) \bar{m}_b \phi_{nb}(x) + \phi_{mm}(x) \bar{m}_m \phi_{nm}(x) + \phi_{mw}(x) \bar{m}_w \phi_{nw}(x)] dx \right\} D_n e^{i\omega_n t} D_m e^{i\omega_n t} (\omega_n^2 - \omega_m^2) = 0 \tag{13}$$

For different natural frequencies $\omega_n^2 \neq \omega_m^2$, the orthogonality condition for different mode shapes of three-beam system is as follows:

$$\begin{cases} \int_0^L [\phi_{mb}(x) \bar{m}_b \phi_{nb}(x) + \phi_{mm}(x) \bar{m}_m \phi_{nm}(x) + \phi_{mw}(x) \bar{m}_w \phi_{nw}(x)] dx = 0, \omega_n \neq \omega_m \\ \int_0^L [\phi_{mb}(x) \bar{m}_b \phi_{nb}(x) + \phi_{mm}(x) \bar{m}_m \phi_{nm}(x) + \phi_{mw}(x) \bar{m}_w \phi_{nw}(x)] dx \neq 0, \omega_n = \omega_m \end{cases} \tag{14}$$

Similar to the solutions of the free transverse vibration shown in Eq. (8), the solutions of the forced transverse vibration can also be assumed in the form shown below:

$$\begin{cases} z_b(x, t) = \sum_{n=1}^{\infty} T_n(t) \phi_{nb}(x) \\ z_m(x, t) = \sum_{n=1}^{\infty} T_n(t) \phi_{nm}(x) \\ z_w(x, t) = \sum_{n=1}^{\infty} T_n(t) \phi_{nw}(x) \end{cases} \tag{15}$$

where $T_n(t)$ is the unknown time function corresponding to the n th natural frequency. The mode shape function has been solved in the free transverse vibration analysis, but $T_n(t)$ needs to be solved.

Substituting Eq. (15) into Eq. (2), Eq. (2) is transformed into the following form:

$$\begin{cases} \bar{m}_b \sum_{n=1}^{\infty} \frac{d^2 T_n(t)}{dt^2} \phi_{nb}(x) + e_b \sum_{n=1}^{\infty} T_n(t) \frac{d^4 \phi_{nb}(x)}{dx^4} + K_{bm} \sum_{n=1}^{\infty} T_n(t) (\phi_{nb}(x) - \phi_{nm}(x)) = f_b(x, t) \\ \bar{m}_m \sum_{n=1}^{\infty} \frac{d^2 T_n(t)}{dt^2} \phi_{nm}(x) + e_m \sum_{n=1}^{\infty} T_n(t) \frac{d^4 \phi_{nm}(x)}{dx^4} - K_{bm} \sum_{n=1}^{\infty} T_n(t) (\phi_{nb}(x) - \phi_{nm}(x)) + K_{mw} \sum_{n=1}^{\infty} T_n(t) (\phi_{nm}(x) - \phi_{nw}(x)) = f_m(x, t) \\ \bar{m}_w \sum_{n=1}^{\infty} \frac{d^2 T_n(t)}{dt^2} \phi_{nw}(x) + e_w \sum_{n=1}^{\infty} T_n(t) \frac{d^4 \phi_{nw}(x)}{dx^4} - K_{mw} \sum_{n=1}^{\infty} T_n(t) (\phi_{nm}(x) - \phi_{nw}(x)) = f_w(x, t) \end{cases} \tag{16}$$

The introduction of free transverse vibration equations can simplify the motion equations of forced transverse vibration. Substituting Eq. (8) into Eq. (10), eliminating the same term $D_n e^{i\omega_n t}$, and multiplying $T_n(t)$ in each term, Eq. (10) is transformed into the following form:

$$\begin{cases} \bar{m}_b \sum_{n=1}^{\infty} \omega_n^2 T_n(t) \phi_{nb}(x) = e_b \sum_{n=1}^{\infty} T_n(t) \frac{d^4 \phi_{nb}(x)}{dx^4} + K_{bm} \sum_{n=1}^{\infty} T_n(t) (\phi_{nb}(x) - \phi_{nm}(x)) \\ \bar{m}_m \sum_{n=1}^{\infty} \omega_n^2 T_n(t) \phi_{nm}(x) = e_m \sum_{n=1}^{\infty} T_n(t) \frac{d^4 \phi_{nm}(x)}{dx^4} \\ K_{bm} \sum_{n=1}^{\infty} T_n(t) (\phi_{nb}(x) - \phi_{nm}(x)) + K_{mw} \sum_{n=1}^{\infty} T_n(t) (\phi_{nm}(x) - \phi_{nw}(x)) \\ \bar{m}_w \sum_{n=1}^{\infty} \omega_n^2 T_n(t) \phi_{nw}(x) = e_w \sum_{n=1}^{\infty} T_n(t) \frac{d^4 \phi_{nw}(x)}{dx^4} - K_{mw} \sum_{n=1}^{\infty} T_n(t) (\phi_{nm}(x) - \phi_{nw}(x)) \end{cases} \tag{17}$$

Substituting Eq. (17) into Eq. (16), the following could be obtained,

$$\begin{cases} \sum_{n=1}^{\infty} \left[\bar{m}_b \phi_{nb}(x) \frac{d^2 T_n(t)}{dt^2} + \bar{m}_b \omega_n^2 \phi_{nb}(x) T_n(t) \right] = f_b(x, t) \\ \sum_{n=1}^{\infty} \left[\bar{m}_m \phi_{nm}(x) \frac{d^2 T_n(t)}{dt^2} + \bar{m}_m \omega_n^2 \phi_{nm}(x) T_n(t) \right] = f_m(x, t) \\ \sum_{n=1}^{\infty} \left[\bar{m}_w \phi_{nw}(x) \frac{d^2 T_n(t)}{dt^2} + \bar{m}_w \omega_n^2 \phi_{nw}(x) T_n(t) \right] = f_w(x, t) \end{cases} \tag{18}$$

We multiply the three terms in Eq. (18) by $\phi_{mb}(x)$, $\phi_{mm}(x)$, and $\phi_{mw}(x)$, respectively. Then, it is integrated with respect to x from 0 to L , and orthogonality condition is applied in Eq. (14), and then, the following could be obtained:

$$\frac{d^2 T_n(t)}{dt^2} + \omega_n^2 T_n(t) = \frac{\int_0^L [\phi_{nb}(x) f_b(x, t) + \phi_{nm}(x) f_m(x, t) + \phi_{nw}(x) f_w(x, t)] dx}{\int_0^L [\phi_{nb}(x) \bar{m}_b \phi_{nb}(x) + \phi_{nm}(x) \bar{m}_m \phi_{nm}(x) + \phi_{nw}(x) \bar{m}_w \phi_{nw}(x)] dx} \tag{19}$$

The unknown time function $T_n(t)$ can be solved by Eq. (19), and the forced transverse vibration response can be obtained by substituting $T_n(t)$ into Eq. (15).

2.1.2 Model comparison and verification

Sun et al. [23, 24] simplified the rolls system of a four-high rolling mill to a simply supported double-beam system, as shown in Fig. 3, and used the analytical method to solve the rolls system transverse bending vibration. The analytical method assumes that, at each natural frequency, the mode shape function of the work roll is a multiple of that of the backup roll.

The process mentioned above for solving the transverse bending vibration of the three-beam system is also suitable for solving the transverse bending vibration of the double-beam system. Therefore, based on the structural parameters of the four-high rolling mill in the reference [23, 24], as shown in Table 1, the natural frequencies ω_n and parameter a are derived using the semi-analytical method and compared with the results solved by analytical

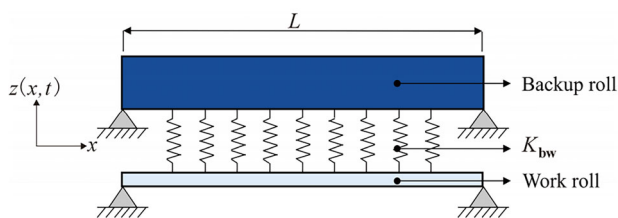


Fig. 3 Rolls system transverse bending vibration model of four-high rolling mill

Table 1 Rolls system structural parameters of four-high rolling mill

L/mm	D_w/mm	D_b/mm	$\rho_w, \rho_b/(\text{kg m}^{-3})$	E/Pa
2030	615	1550	7.8×10^3	2.1×10^{11}

Table 2 Comparison between semi-analytical method and analytical method

ω_n/Hz		a	
Analytical method [23, 24]	Semi-analytical method	Analytical method [23, 24]	Semi-analytical method
4237.1	4250.7	2.2	2.256
6204.5	6224.4	-2.8154	-2.81475
9132.8	9162.2	71.4	71.404
17,874.1	17,931.3	382.8	381.962
19,315.1	19,376.9	-0.0889	-0.08887

method to verify the correctness of the model. The comparison results are shown in Table 2.

As shown in Table 2, ω_n and a solved by two methods are very close to each other, which verifies the correctness of the semi-analytical method for solving the rolls system transverse bending vibration. In addition, the semi-analytical method eliminates the need to assume the shape mode function relationship between adjacent rolls. It can be further applied to the solution of rolls system transverse vibration of six-high rolling mill rather than just four-high rolling mill, making it more widely applicable.

2.2 Roll vertical chatter model

2.2.1 Model construction

The roll vertical chatter model has been established in our previous work [35]. The vertical chatter model combines the structural dynamic model with the dynamic rolling process model, and a critical rolling speed for chatter instability is proposed. The modeling process is as follows:

Firstly, for six-high rolling mill, eight-degree-of-freedom structural dynamic model is established:

$$M\ddot{Y} + C\dot{Y} + KY = F_{\text{var}} \tag{20}$$

where M , C , and K are the mass matrix, damping matrix, and stiffness matrix; Y is the displacement vector; \dot{Y} is the velocity vector; \ddot{Y} is the accelerator vector; F_{var} is the force vector and $F_{\text{var}} = [0, 0, 0, P_{\text{var}}, -P_{\text{var}}, 0, 0, 0]^T$; and P_{var} is the dynamic rolling force. Ignoring the dynamic fluctuation of entry thickness and rolling speed, P_{var} can be figured by:

$$P_{\text{var}} = F_1 \dot{h}_{c,\text{var}} + F_2 h_{c,\text{var}} + F_3 \sigma_{\text{xe},\text{var}} + F_4 \sigma_{\text{xd},\text{var}} \tag{21}$$

where $h_{c,\text{var}}$ is the dynamic variation in roll gap; $\dot{h}_{c,\text{var}}$ is the change rate of $h_{c,\text{var}}$; $\sigma_{\text{xd},\text{var}}$ is the dynamic front tension; $\sigma_{\text{xe},\text{var}}$ is the dynamic back tension; and F_s ($s = 1-4$) is the influential coefficient of dynamic rolling force. The tension is also influenced by variation in roll gap:

$$\begin{cases} \dot{\sigma}_{\text{xe},\text{var}} = E(G_1 \dot{h}_{c,\text{var}} + G_2 h_{c,\text{var}})/l \\ \dot{\sigma}_{\text{xd},\text{var}} = -E(G_3 \dot{h}_{c,\text{var}} + G_4 h_{c,\text{var}})/l \end{cases} \tag{22}$$

where l is the distance between adjacent stands; and G_s ($s = 1-4$) is the influential coefficient of dynamic front and back tension.

Then, combining Eqs. (21) and (22) into Eq. (20), the following state equation is obtained.

$$\dot{z} = J \cdot z(t) \tag{23}$$

where $z = [y_r, \dot{y}_r, \sigma_{\text{xe},\text{var}}, \sigma_{\text{xd},\text{var}}]^T$ ($r = 1-8$); y_r and \dot{y}_r are the rolls dynamic displacement and velocity; \dot{z} is the change rate of z ; and J is the matrix of state equation. Applying Laplace transformation on Eq. (23), the s -domain model is expressed as follows:

$$A_z \cdot Z(s) = 0 \tag{24}$$

where A_z is the coefficient matrix; and $Z(s)$ is the state vector after Laplace transformation. Finally, when the condition of characteristic equation is satisfied, i.e., the coefficient matrix $|A_z| = 0$, the critical rolling speed can be calculated by the Routh stability criterion.

2.2.2 Model verification

Taking the six-high rolling mill of the fifth stand in the cold tandem mill as an example, the actual production data are collected through vibration monitoring system, as shown in Fig. 4. The vibration acceleration signals are collected by the piezoelectric sensors with 5120-Hz sampling frequency, which are installed on the upper stands. The data of rolling speed and vibration acceleration for a coin of steel product are demonstrated in Fig. 5, in which chatter can be evidently observed.

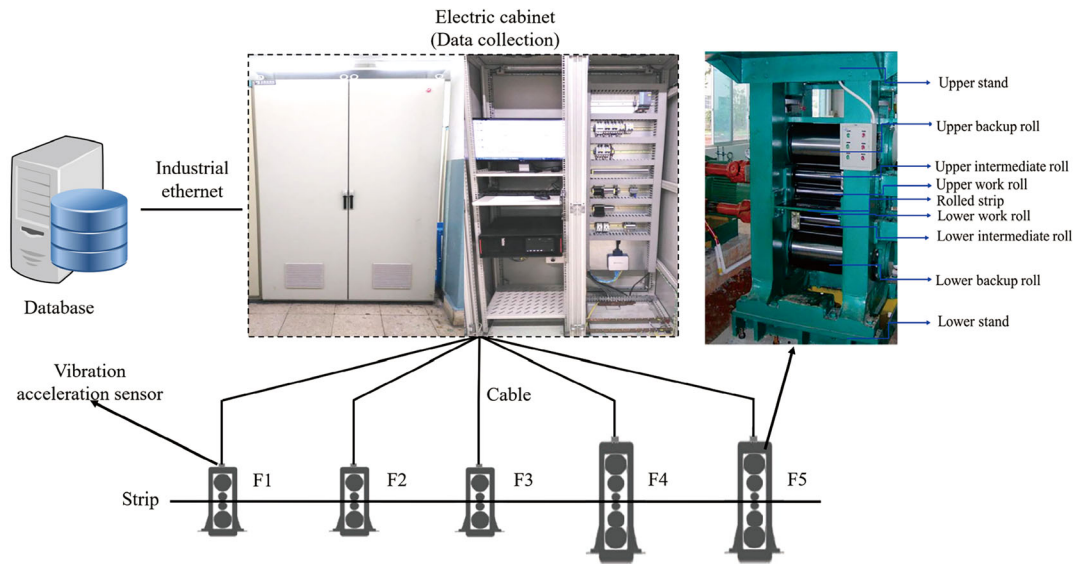


Fig. 4 Vibration monitoring system

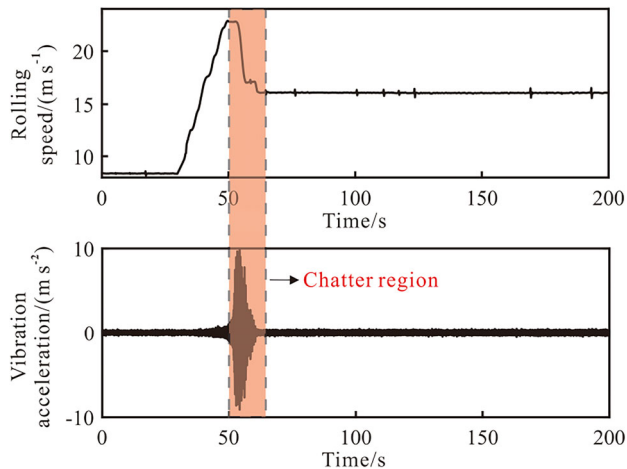


Fig. 5 Rolling speed and vibration acceleration signals for a coil of steel product

For the picked chatter region shown in Fig. 5, the critical rolling speed equals to 22.67 m s^{-1} , and experimental results and model-based calculation are compared in Fig. 6. According to Fig. 6, both experimental and simulation results show that the chatter occurs when the rolling speed is over the calculated critical speed, and chatter can be effectively suppressed by decreasing the rolling speed. In addition, the simulated vibration frequencies are also close to the experimental one. The above analysis verifies the correctness of the roll vertical chatter model.

The rigid-flexible coupling vibration model of rolls system is established through the coupling of the above transverse bending vibration model and vertical chatter model. Both transverse bending vibration and vertical chatter occur in the rolls system under the action of

dynamic rolling force, where the transverse bending vibration reflects the flexible deformation of the rolls system, and the vertical chatter reflects the rigid movement of the rolls system. Both of these effects affect the size and shape of the roll gap and then affect the strip exit thickness. The coupling form of transverse bending vibration and vertical chatter is shown in Fig. 7.

The roll vertical chatter model provides exciting force for the rolls system transverse bending vibration model, that is, P_{var} shown in Eq. (21), which is used to determine $T_n(t)$ shown in Eq. (19). Using the critical rolling speed in roll vertical chatter model, the dynamic characteristics of rolls system under stable and unstable rolling processes can be further explored. The rolls system transverse bending vibration model can obtain the transverse deflection of rolls and the distribution of strip exit thickness along the width direction, which compensates for the limitation of the vertical chatter model. The rigid-flexible coupling vibration model calculation process is shown in Fig. 8. Δt is the increment of time at each cycle, and t_{set} is the set value of cycle time.

3 Rolls system dynamic characteristics

Taking the six-high rolling mill of the fifth stand in Fig. 4 as the research object, the rolls system structural parameters and rolling process parameters under a typical working condition are shown in Tables 3 and 4, respectively.

The first nine modes shape function of the rolls system transverse vibration is solved based on the structural parameters in Table 3, as shown in Fig. 9.

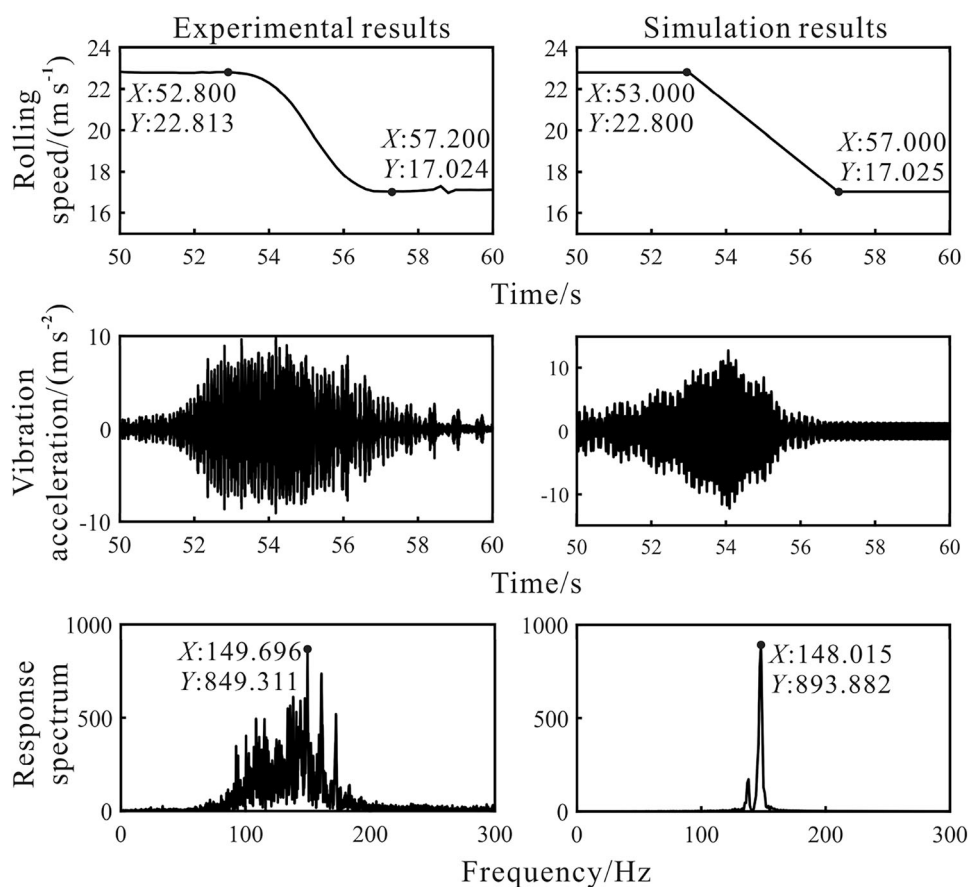


Fig. 6 Comparison of experimental and simulation results

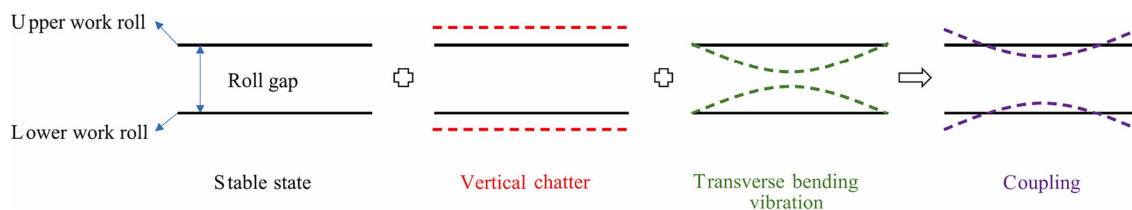


Fig. 7 Coupling form of transverse bending vibration and vertical chatter

The displacements of both ends of the rolls are limited by simply supported boundary conditions. The mode shape function gradually transitions from quadratic polynomial to a higher order polynomial, and even with the same type of mode shape function, there are different characteristics. In Fig. 9a, the vibration directions of the work roll, intermediate roll, and backup roll are the same. The transverse deflection of the work roll is the largest, and the transverse deflection of the intermediate roll is larger than that of the backup roll. In Fig. 9b, the vibration direction of the work roll is opposite to that of the intermediate roll and backup roll, and the transverse deflection of the backup roll is larger than that of the intermediate roll. Mode shape functions can be divided into two categories: One concerns

z -directional symmetry, and the other concerns roll center point symmetry.

As shown in Table 4, the rolling speed is 22 m s^{-1} , which is lower than the critical rolling speed. Thus, the rolls system is in a stable state, and the dynamic rolling force generated by the vertical chatter is taken as exciting force of the rolls system transverse bending vibration. According to the calculation process shown in Fig. 8, the work roll forced transverse vibration responses corresponding to each mode are obtained, as shown in Fig. 10.

In Fig. 10, the work roll transverse deflection under the mode shape function with z -directional symmetry is much larger than that under the mode shape function with roll center point symmetry. In addition, even under the same type of mode shape function, with the increase in the mode

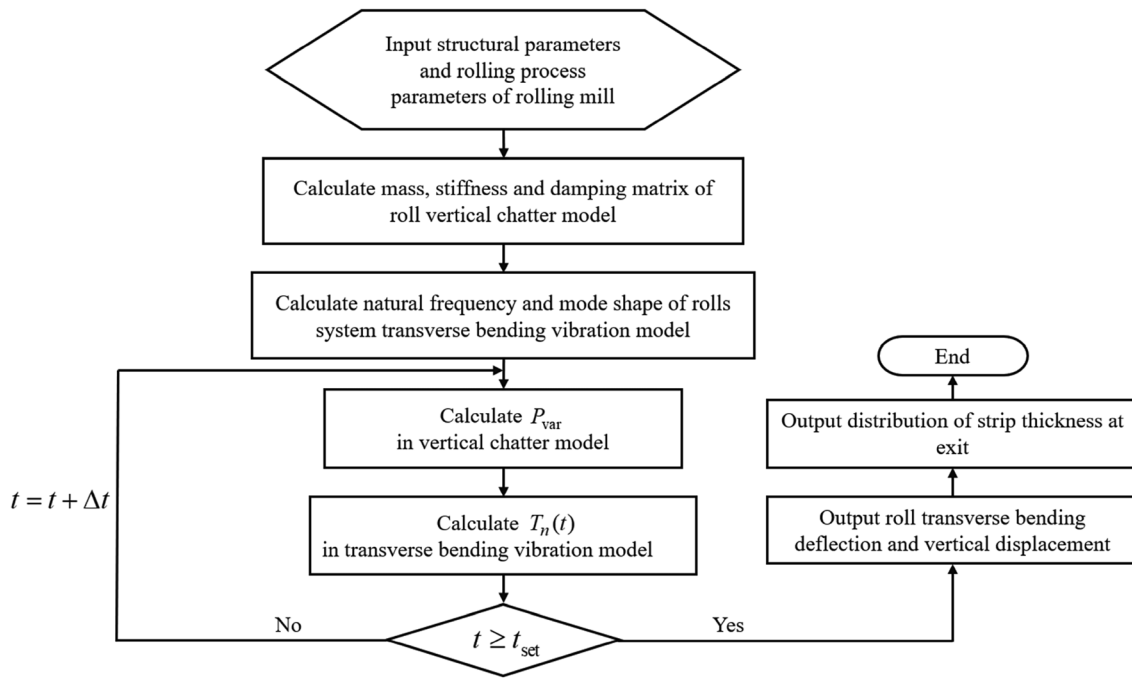


Fig. 8 Flowchart of rigid-flexible coupling vibration model calculation process

Table 3 Rolls system structural parameters of six-high rolling mill

Parameter	Value	Parameter	Value
L/mm	1420	D_b/mm	1200
D_w/mm	400	$\rho_w, \rho_m, \rho_b/(kg\ m^{-3})$	7.8×10^3
D_m/mm	500	E/Pa	2.1×10^{11}

Table 4 Rolling process parameters

Parameter	Value	Parameter	Value
Strip width B/mm	1048	Front tension σ_{xd}/MPa	60
Entry thickness h_e/mm	0.305	Friction coefficient f	0.02
Exit thickness h_c/mm	0.202	Rolling speed $v_r/(m\ s^{-1})$	22
Back tension σ_{xc}/MPa	156	Critical rolling speed $v_{rc}/(m\ s^{-1})$	23.84

order, the work roll transverse deflection will gradually decrease, as shown in Fig. 10a, b, and d.

The work roll forced transverse vibration responses under the first nine modes are superimposed, and the superimposed transverse deflections at the midpoint of different rolls are analyzed, as shown in Fig. 11. The

transverse vibration curve of work roll is mainly quadratic polynomial curve, and compared with the intermediate roll and the backup roll, the transverse deflection of the work roll is the largest because the work roll is directly affected by the dynamic rolling force.

4 Strip exit thickness distribution under different rolling processes

When the actual rolling speed is lower than the critical rolling speed, the rolls system is under stable rolling process, and the strip exit thickness fluctuation caused by the roll vertical chatter will gradually converge with time, as shown in Fig. 12a. Therefore, under the stable rolling process, the main reason for fluctuation is the rolls system transverse bending vibration.

When the actual rolling speed exceeds the critical rolling speed, the rolls system is under unstable rolling process, and the strip exit thickness fluctuation caused by the roll vertical chatter rapidly diverges in a short time, as shown in Fig. 12b. At the same time, the dynamic rolling force gradually increases to diverge, resulting in more severe rolls system transverse bending vibration. Thus, under the unstable rolling process, the strip exit thickness fluctuation is caused by the combined influence of rolls system vertical chatter and transverse bending vibration.

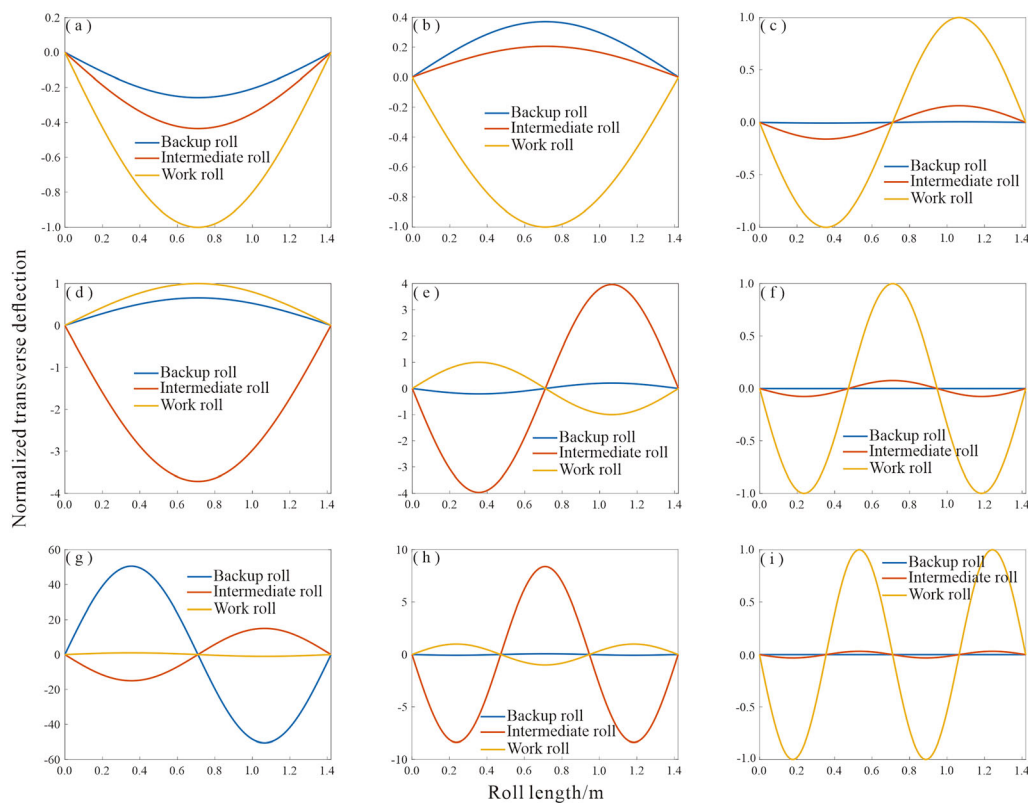


Fig. 9 First nine modes shape function of rolls system transverse bending vibration. **a** 1st shape function; **b** 2nd shape function; **c** 3rd shape function; **d** 4th shape function; **e** 5th shape function; **f** 6th shape function; **g** 7th shape function; **h** 8th shape function; **i** 9th shape function

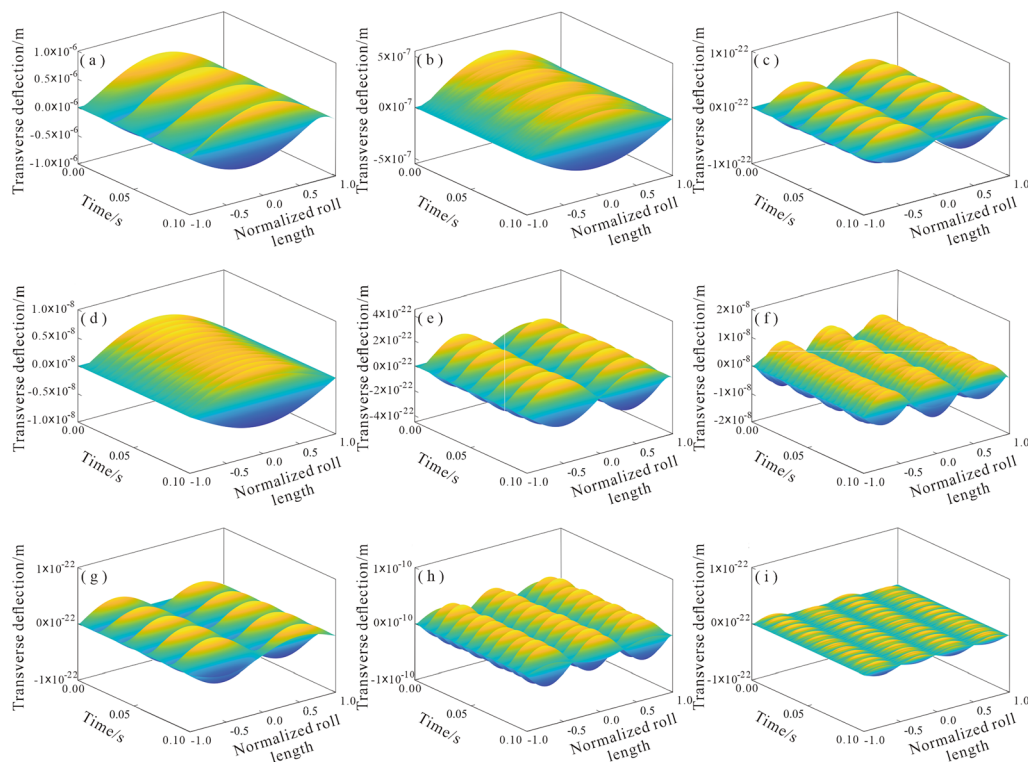


Fig. 10 Work roll forced transverse vibration response under different modes. **a** 1st mode; **b** 2nd mode; **c** 3rd mode; **d** 4th mode; **e** 5th mode; **f** 6th mode; **g** 7th mode; **h** 8th mode; **i** 9th mode

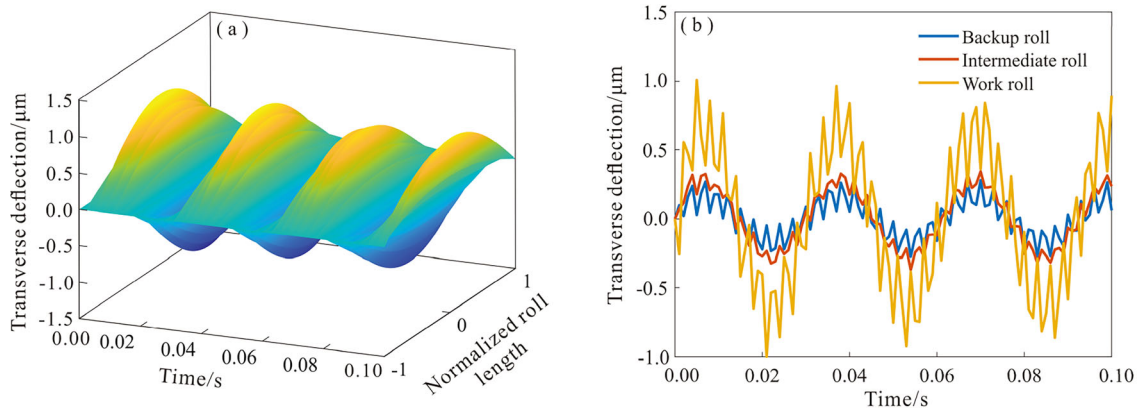


Fig. 11 Rolls system transverse vibration response after superposition. **a** Work roll forced transverse vibration response; **b** rolls system transverse deflections at midpoint

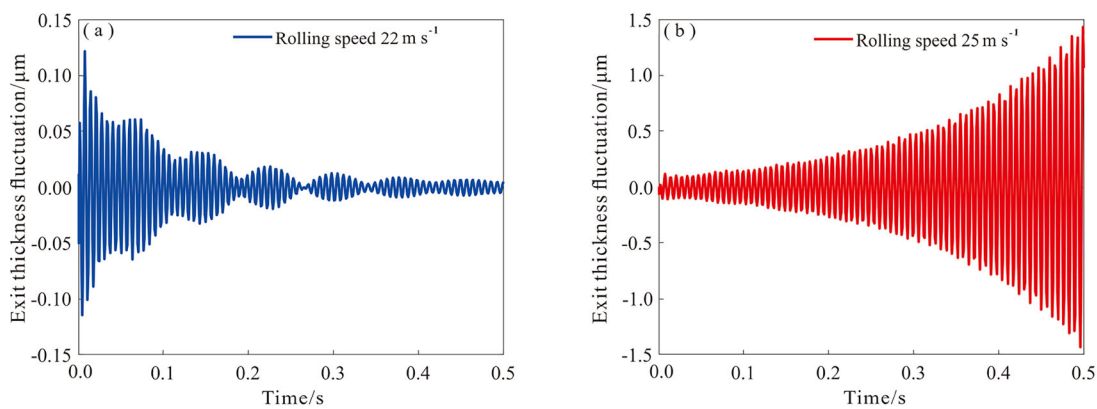


Fig. 12 Strip thickness fluctuation caused by roll vertical chatter. **a** Stable rolling process; **b** unstable rolling process

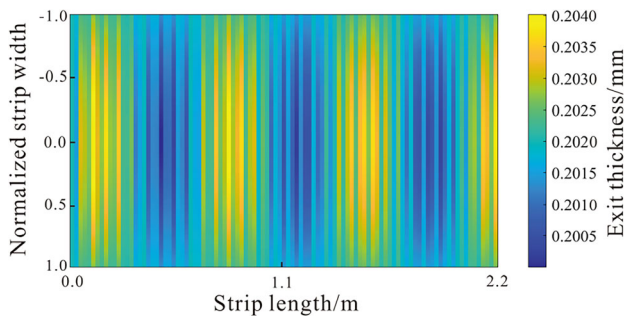


Fig. 13 Strip exit thickness distribution under stable rolling process

4.1 Strip exit thickness distribution under stable rolling process

Taking the typical working condition shown in Tables 3 and 4 as an example, the rolling speed is 22 m s^{-1} , and the rolling process is in the stable state. The length of the strip is calculated by multiplying the simulation time and the rolling speed. The strip exit thickness distribution caused by the rolls system transverse bending vibration is obtained as shown in Fig. 13.

To further verify the correctness of the model, the strip exit thickness was measured. The experimental and simulation results of the exit thickness at the position of strip midpoint are compared in Fig. 14. The simulation result is basically consistent with the experimental result. The simulated and measured exit thicknesses fluctuate around the set value of 0.202 mm , and the fluctuation range is $\pm 2 \text{ }\mu\text{m}$. Therefore, under a stable rolling process, the transverse bending vibration of rolls system is one of the reasons for the change of the strip exit thickness along the rolling direction.

Assuming that the cross-section of the strip is shown in Fig. 15, the crown is an important index used to measure the cross-section of the strip, reflecting the strip transverse thickness difference between the midpoint and the marked point at the edge, as shown in Eq. (25).

$$C_x = h_0 - \frac{h_1 + h_2}{2} \tag{25}$$

where h_0 is the strip thickness at the strip midpoint; h_1 is the strip thickness at the strip edge marked point of operate side; h_2 is the strip thickness at the strip edge marked point

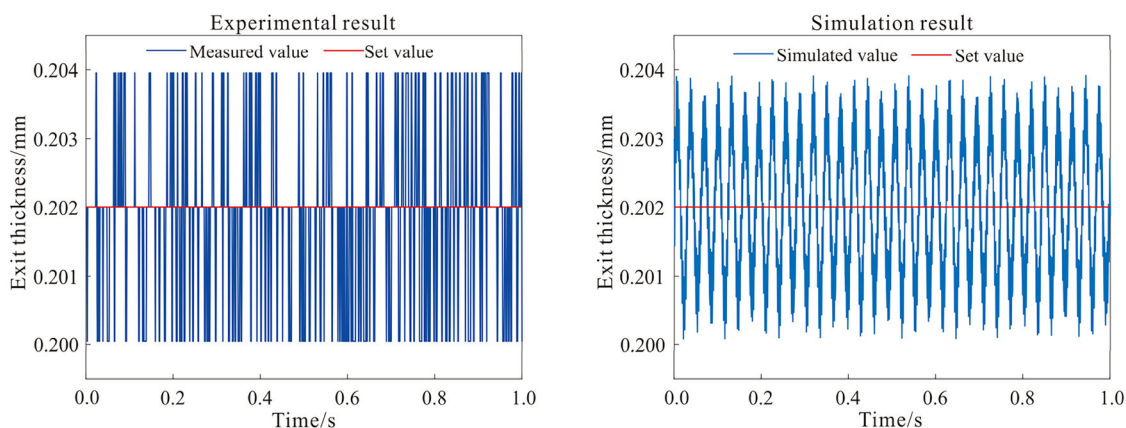


Fig. 14 Comparison of simulated and measured exit thickness at position of strip midpoint

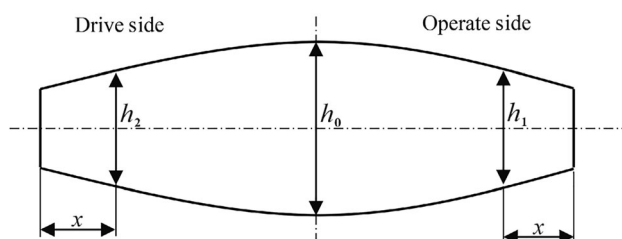


Fig. 15 Cross-section of strip

of drive side; and x is the distance between the strip edge and the marked points of drive side and operate side.

To further quantify the strip thickness distribution shown in Fig. 13, the crown C_{40} is used to measure the strip transverse thickness difference, and the maximum longitudinal thickness difference of each position along the strip width direction is used to measure the longitudinal thickness difference, as shown in Fig. 16. Under stable rolling process, the absolute value of the maximum crown caused by the rolls system transverse bending vibration can reach $1.13 \mu\text{m}$, and the maximum

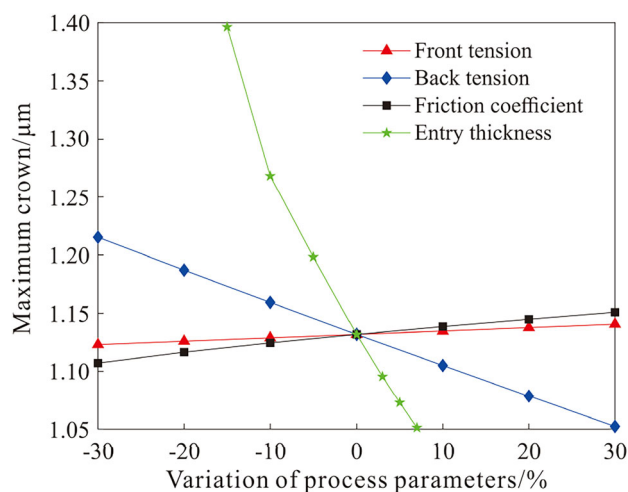


Fig. 17 Relationship between maximum crown and variation of process parameters

longitudinal thickness difference occurs at the midpoint of the strip, which can reach $4 \mu\text{m}$. The strip thickness difference does not show a divergent trend.

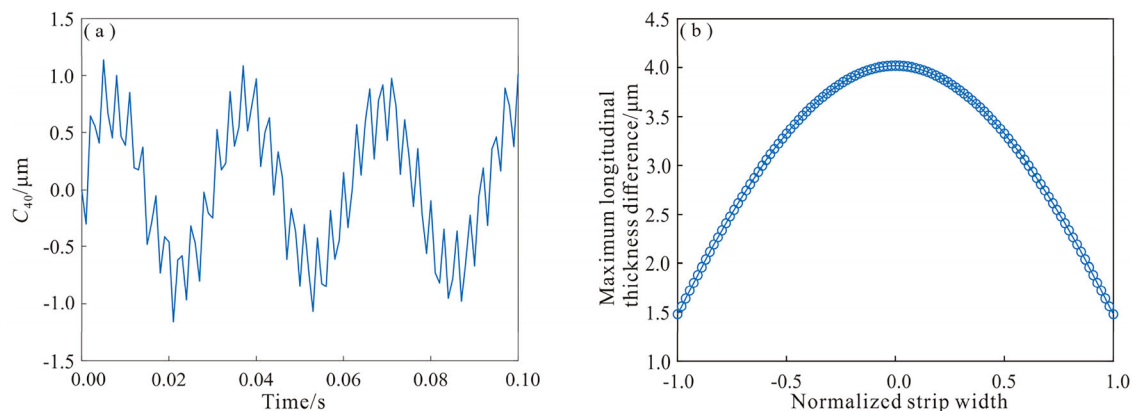


Fig. 16 Transverse and longitudinal thickness difference of strip under stable rolling process. **a** Crown; **b** maximum longitudinal thickness difference

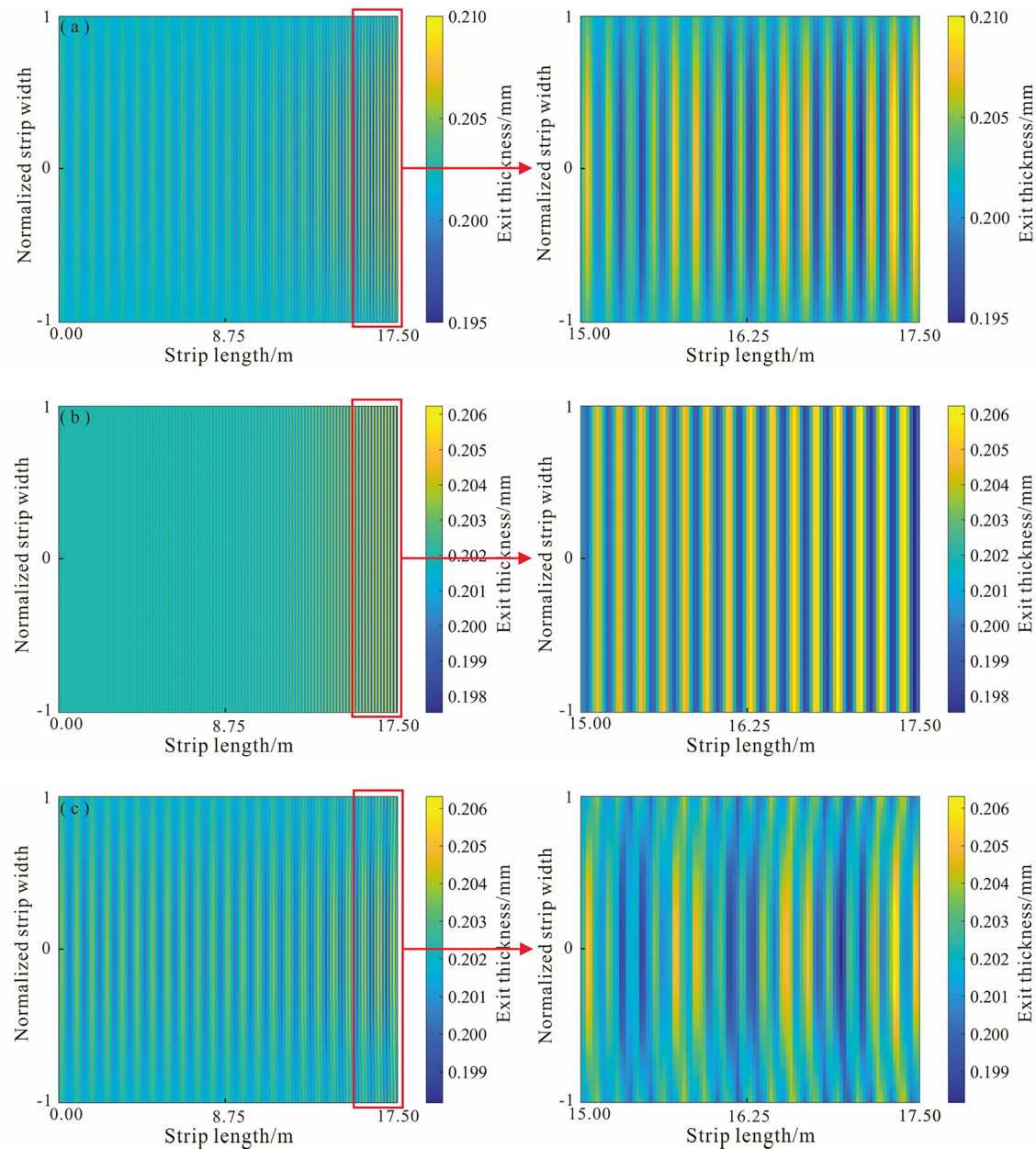


Fig. 18 Strip exit thickness distribution under unstable rolling process. **a** Effect of rolls system transverse bending vibration; **b** effect of roll vertical chatter; **c** combined effect of transverse bending vibration and vertical chatter

Under stable rolling process, the variation of the dynamic rolling force caused by the variation of the process parameters will lead to the variation of the forced transverse vibration response of the rolls system, which will change the strip crown. Therefore, based on the process parameters in Table 4, the relationship between the maximum crown caused by transverse vibration and the variation of process parameters is studied, as shown in Fig. 17. The front tension and friction coefficient are

positively correlated with the maximum crown, while the back tension and entry thickness are negatively correlated with the maximum crown. The change of the entry thickness has the greatest influence on the maximum crown. When the entry thickness increases, the strip crown caused by the rolls system transverse bending vibration will obviously decrease. However, when the entry thickness increases by 7%, the critical rolling speed is lower than 22 m s^{-1} , and the rolls system will enter an unstable state.

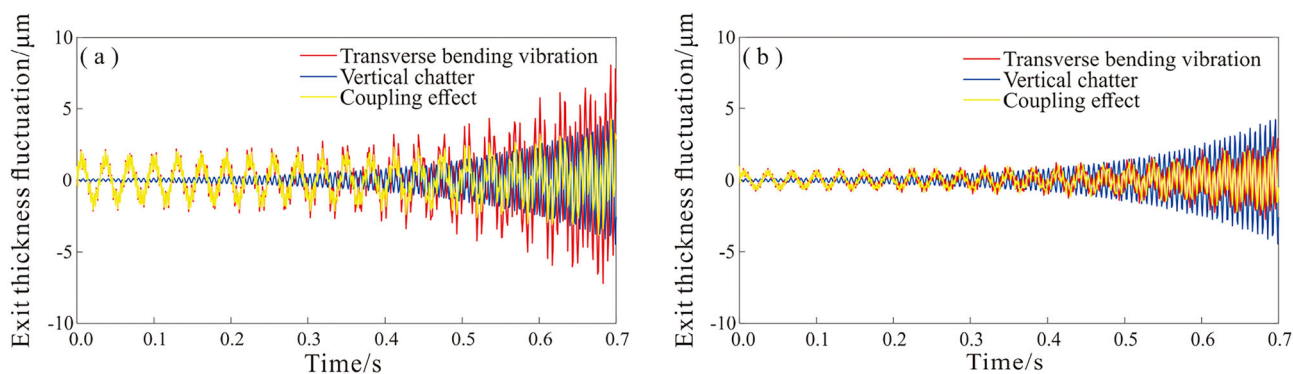


Fig. 19 Exit thickness fluctuation at position of strip midpoint and endpoint. **a** Strip midpoint; **b** strip endpoint

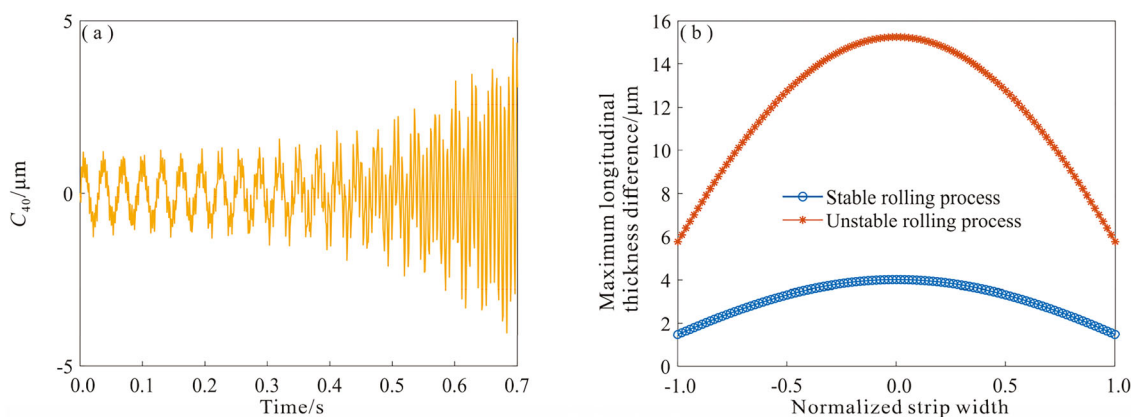


Fig. 20 Transverse and longitudinal thickness difference of strip under unstable rolling process. **a** Crown; **b** maximum longitudinal thickness difference

4.2 Strip exit thickness distribution under unstable rolling process

The rolling speed is set to 25 m s^{-1} to simulate the unstable rolling process, and strip exit thickness distribution under the combined influence of rolls system transverse bending vibration and vertical chatter is obtained, as shown in Fig. 18.

In Fig. 18a, rolls system transverse bending vibration causes both the longitudinal and transverse thickness differences of the strip, and in Fig. 18b, roll vertical chatter mainly causes the longitudinal thickness difference of the strip. As shown in Fig. 18c, with the continuation of the unstable rolling process, the strip thickness fluctuation gradually shows a divergent trend. In order to further analyze the influence of rolls system transverse bending vibration and vertical chatter on strip exit thickness, the positions of the midpoint and endpoint of strip are selected for analysis, as shown in Fig. 19. Compared with the position of endpoint, the fluctuation amplitude of the strip thickness at the midpoint is more intense. In addition, at the position of endpoint, the thickness fluctuation caused by the vertical chatter is greater than that caused by the transverse bending vibration,

but it is just the opposite at the position of midpoint. And the strip thickness fluctuation caused by transverse bending vibration and vertical chatter will be offset to a certain extent, but it still shows a divergent trend.

As shown in Fig. 20, under the unstable rolling process, the crown shows a divergent trend, that is, the transverse thickness difference of the strip will gradually diverge with time. In addition, the maximum longitudinal thickness difference under the unstable rolling process is larger than that under the stable rolling process. Therefore, in the process of unstable rolling, there will be not only the longitudinal thickness difference caused by roll vertical chatter, but also the transverse thickness difference caused by rolls system transverse bending vibration.

5 Conclusions

Vertical chatter and transverse bending vibration of the rolls system will lead to strip longitudinal and transverse thickness difference, flatness defects, and rolling process instability. Therefore, considering the influence of rolls system deformation and movement, the rolls system transverse

bending vibration model described by partial differential equations and the roll vertical chatter model described by ordinary differential equations are established, and the correctness of the models are verified by comparing with the previous works and the experimental results, respectively. Then, the rigid-flexible coupling vibration model of the rolls system is established by coupling of the vertical chatter model and transverse bending vibration model through the transverse distribution of dynamic rolling force, and the dynamic characteristics of rolls system and strip exit thickness distribution are analyzed.

Under the stable rolling process, the strip exit thickness fluctuation is mainly caused by the rolls system transverse bending vibration. The maximum crown can reach 1.13 μm , and the maximum longitudinal thickness difference can reach 4 μm . Under the unstable rolling process, the strip exit thickness fluctuation caused by rolls system vertical chatter and transverse bending vibration should be taken into account comprehensively. At the position of strip endpoint, the thickness fluctuation caused by the vertical chatter is greater than that caused by the transverse bending vibration, but it is just the opposite at the position of strip midpoint, and both show a divergent trend.

In this paper, the rolls system transverse bending vibration under simply supported boundary conditions is mainly analyzed. Compared with the analytical method in the previous work, the semi-analytical method used to solve the rolls system transverse bending vibration has a wider range of application. It is not only suitable for different types of rolling mills, but also can solve the transverse bending vibration under different boundary conditions. It is only necessary to form different boundary conditions coefficient matrix. Therefore, in the future work, the dynamic characteristics of the rolls system under different boundary conditions such as free or spring supported can be further analyzed.

Acknowledgements This work was supported by the National Natural Science Foundation of China (No. 51775038).

Declarations

Conflict of interest The authors declare that they have no conflict of interest concerning the publication of this manuscript.

References

- [1] R.M. Guo, A.C. Urso, J.H. Schunk, *Iron Steel Eng.* 70 (1993) 29–39.
- [2] M.R. Niroomand, M.R. Forouzan, M. Salimi, H. Shojaei, *ISIJ Int.* 52 (2012) 2245–2253.
- [3] Y.D. Kim, C.W. Kim, S.J. Lee, H.J. Park, *ISIJ Int.* 52 (2012) 2042–2047.
- [4] Y.J. Zheng, G.X. Shen, Y.G. Li, M. Li, H.M. Liu, *J. Iron Steel Res. Int.* 21 (2014) 837–843.
- [5] R. Mehrabi, M. Salimi, S. Ziaei-Rad, *J. Manuf. Sci. Eng.* 137 (2015) 061013.
- [6] M. Mosayebi, F. Zarrinkolah, K. Farmanesh, *Int. J. Adv. Manuf. Technol.* 91 (2017) 4359–4369.
- [7] D.K. Lee, J. Nam, J.S. Kang, J.S. Chung, S.W. Cho, *Int. J. Adv. Manuf. Technol.* 94 (2018) 4459–4467.
- [8] X. Liu, Y. Zang, Z. Gao, L. Zeng, *Shock. Vib.* 2016 (2016) 1–15.
- [9] L. Zeng, Y. Zang, Z. Gao, *J. Vib. Acoust.* 139 (2017) 061015.
- [10] Z.Y. Gao, Y. Liu, Q.D. Zhang, M.L. Liao, B. Tian, *Mech. Syst. Signal Process.* 140 (2020) 106692.
- [11] X. Lu, J. Sun, G. Li, Q. Wang, D. Zhang, *J. Mater. Process. Technol.* 272 (2019) 47–57.
- [12] Z.Y. Gao, B. Tian, Y. Liu, L.Y. Zhang, M.L. Liao, *J. Iron Steel Res. Int.* 28 (2021) 168–180.
- [13] A. Heidari, M.R. Forouzan, S. Akbarzadeh, *ISIJ Int.* 54 (2014) 165–170.
- [14] N. Fujita, Y. Kimura, K. Kobayashi, K. Itoh, Y. Amanuma, Y. Sodani, *J. Mater. Process. Technol.* 229 (2016) 407–416.
- [15] L. Cao, X. Li, Q. Wang, D. Zhang, *Tribol. Int.* 153 (2021) 106604.
- [16] M.D. Stone, R. Gray, *Iron Steel Eng.* 42 (1965) 73–90.
- [17] K.N. Shohet, N.A. Townsend, *Tetsu-to-Hagane* 206 (1968) 1088–1098.
- [18] C.Y. He, Z.J. Jiao, X.J. Wang, *Adv. Mater. Res.* 700 (2013) 98–102.
- [19] H. Zhou, J.L. Bai, *Appl. Mech. Mater.* 633–634 (2014) 791–794.
- [20] D.C. Tran, N. Tardif, A. Limam, *Int. J. Solids Struct.* 69–70 (2015) 343–349.
- [21] X.L. Chen, J.X. Zou, in: *Proceedings of the 4th International Steel Rolling Conference*, Deauville, France, 1987, pp. E4.1–E4.7.
- [22] Q. Yang, X.L. Chen, Y.H. Xu, L.J. Xu, *Iron Steel* 30 (1995) No.2, 48–51.
- [23] J.L. Sun, *Dynamic model building of rolling mill system for thickness and shape control of strip*, Yanshan University, Qinhuangdao, China, 2010.
- [24] J.L. Sun, Y. Peng, H.M. Liu, G.B. Jiang, *J. Cent. South Univ.* 40 (2009) 429–435.
- [25] J.L. Sun, Y. Peng, H.M. Liu, G.B. Jiang, *J. Cent. South Univ. Technol.* 16 (2009) 954–960.
- [26] J.L. Sun, Y. Peng, H.M. Liu, *J. Cent. South Univ.* 21 (2014) 567–576.
- [27] S. Kapil, P. Eberhard, S.K. Dwivedy, *J. Manuf. Sci. Eng.* 138 (2016) 041002.
- [28] A. Malik, *Rolling mill optimization using an accurate and rapid new model for mill deflection and strip thickness profile*, Wright State University, Dayton, USA, 2007.
- [29] A.S. Malik, R.V. Grandhi, *J. Mater. Process. Technol.* 206 (2008) 263–274.
- [30] A.S. Malik, J.L. Hinton, *J. Manuf. Sci. Eng.* 134 (2012) 1.
- [31] F. Zhang, A. Malik, *J. Manuf. Sci. Eng.* 140 (2018) 011008.
- [32] F. Zhang, A.S. Malik, *J. Manuf. Sci. Eng.* 143 (2021) 101005.
- [33] A. Patel, A.S. Malik, F. Zhang, *Int. J. Adv. Manuf. Technol.* 120 (2022) 7389–7413.
- [34] A. Patel, A. Malik, R. Mathews, *J. Manuf. Sci. Eng.* 144 (2022) 071009.
- [35] Z. Gao, *J. Mech. Eng.* 53 (2017) 118.

Springer Nature or its licensor (e.g. a society or other partner) holds exclusive rights to this article under a publishing agreement with the author(s) or other rightsholder(s); author self-archiving of the accepted manuscript version of this article is solely governed by the terms of such publishing agreement and applicable law.